Fluorescence Correlation Spectroscopic Studies of a Single Lipopolyamine–DNA Nanoparticle

CHAPTER · DECEMBER 2007

DOI: 10.1007/4243_2007_014

6 AUTHORS, INCLUDING:

Aleš Benda
University of New South Wales
36 PUBLICATIONS **976** CITATIONS

Springer Ser Fluoresc (2008) 4: 381–413
DOI 10.1007/4243_2007_014

Published online: 13 October 2007

Fluorescence Correlation Spectroscopic Studies of a Single Lipopolyamine–DNA Nanoparticle

Noppadon Adjimatera[1] · Aleš Benda[2] · Ian S. Blagbrough[1] · Marek Langner[3] · Martin Hof[2] · Teresa Kral[2,4] (✉)

[1]Department of Pharmacy and Pharmacology, University of Bath, Bath BA2 7AY, UK

[2]J. Heyrovský Institute of Physical Chemistry, Academy of Sciences of the Czech Republic, Dolejškova 3, 182 23 Prague 8, Czech Republic
kral@jh-inst.cas.cz

[3]Institute of Physics, Wrocław University of Technology, Wybrzeże Wyspiańskiego 27, 50-370 Wrocław, Poland

[4]Department of Physics and Biophysics, Wrocław University of Environmental and Life Sciences, Norwida 25, 50-375 Wrocław, Poland

Abstract We have studied lipopolyamine–DNA complex formation by fluorescence correlation spectroscopy (FCS). Two lipopolyamines, N^4,N^9-dioleoylspermine and N^1-cholesteryl spermine carbamate, were used to condense linear calf thymus DNA and two plasmid DNAs: pGL3 (5.3 kilobase pairs) and pEGFP (4.7 kilobase pairs). PicoGreen® (PG), a high-affinity DNA intercalating agent that only fluoresces when intercalated, was used in our FCS study. In this study, the ConfoCor I set-up upgraded with TimeHarp 200 was used. FCS directly visualizes the condensation process by tracking changes in diffusion coefficients and particle numbers. We were able to define the fluorescent signalling

behaviour of PG through the process from dye binding to dye release and then dye quenching. Dye release was suggested as the indicator for DNA conformational change, but not for nanoparticle formation. Dye quenching, through the observation of lifetime change, is a more important event accurately and sensitively reporting that a single nanoparticle exists.

Keywords DNA condensation · FCS · Fluorescent lipopolyamines · Non-viral gene therapy · PicoGreen · Polyamines · TTTR data

Abbreviations

A	Correction factor
C	Molarity
CR	Count rate
ct DNA	Calf thymus DNA
D	Diffusion coefficient
DNA	Deoxyribonucleic acid
DNase	Nuclease
dsDNA	Double-stranded DNA
EthBr	Ethidium bromide
F_0	Fluorescence intensity in the absence of quencher
F_q	Fluorescence intensity in the presence of quencher
FCS	Fluorescence correlation spectroscopy
$G(\tau)$	Autocorrelation function
HEPES	4-(2-Hydroxyethyl)-1-piperazine-ethanesulphonic acid
k_B	Boltzmann constant
M	Molecular mass
N/P	Ammonium/phosphate ratio
N_A	Avogadro's number
NaCl	Sodium chloride
NVGT	Non-viral gene therapy
η	Dynamic viscosity
pEGFP	pEGFP plasmid DNA
PG	PicoGreen®
pGL3	pGL3 plasmid DNA
PN	Particle number
r_h	Hydrodynamic radius
ssDNA	Single-stranded DNA
τ	Correlation time
τ_D	Diffusion time
τ_0	Lifetime of the fluorophore in the absence of quencher
τ_q	Lifetime of the fluorophore in the presence of quencher
τ_{tr}	Triplet decay time
T	Triplet fraction
T_C	Thermodynamic temperature
TCSPC	Time-correlated single photon counting
TTTR	Time-tagged time-resolved
V	Confocal volume
ω_1	Lateral radius of detection volume
ω_2	Axial radius of detection volume
χ	Fit parameter

1 Introduction

DNA binding by lipopolyamines plays an important role in gene delivery success. DNA condensation affords nanoparticles with the appropriate size to enter cells, as well as giving protection from nucleases (DNases), and these are important properties when considering serum stability for in vivo applications. Disassociation of DNA at the right time is crucial, possibly after escaping from the endosome and just before reaching or right after entering a nucleus. However, the association and dissociation between these lipopolyamines and DNA are still not well understood [1–7].

Fluorescence correlation spectroscopy (FCS) is a relatively new non-invasive technique with single-molecule sensitivity to study molecular diffusion, large conformational changes and molecular interactions based on fluorescence and confocal microscopy. In conventional fluorescence spectroscopy, a relatively large volume of sample is illuminated by an excitation light. Thus, the fluorescence signal is recorded from the whole ensemble of molecules leading to averaged information. The single-molecule sensitivity of fluorescence confocal microscopy overcomes this limitation and provides non-averaged information about the sample. FCS was used to study the dynamic processes on the molecular scale, including DNA nanoparticle formation [8–14]. One advantage of the FCS approach is that it works at low concentrations (difficult to attain by other technologies) and consequently opens measurement possibilities at physiologically relevant levels.

2 Principles of Fluorescence Correlation Spectroscopy

Fluorescence approaches, like ethidium bromide (EthBr) quenching during DNA condensation [15] and DNA detection on gels using EthBr, are among many commonly used bulky fluorescence techniques applied in non-viral gene therapy (NVGT) research. Their advantage is simplicity; on the other hand they require rather large amounts of sample and provide only averaged information about the system. Decreasing the effective detection volume to femtolitre size (Fig. 1) by using confocal optics and nanomolar concentrations of samples bring us to a single-molecule level. This opens new dimensions in the NVGT research field. Standard fluorescence parameters (spectra, lifetime, anisotropy) can be obtained in a non-averaged, molecule by molecule, evaluated manner. Moreover, changes in local concentrations and brightness of the studied molecules due to diffusion, chemical reactions, photophysical events and other effects lead to pronounced fluctuations in the overall detected fluorescence intensity. Thus, the temporal evolution of the detected fluorescence intensity carries information about concentrations, dif-

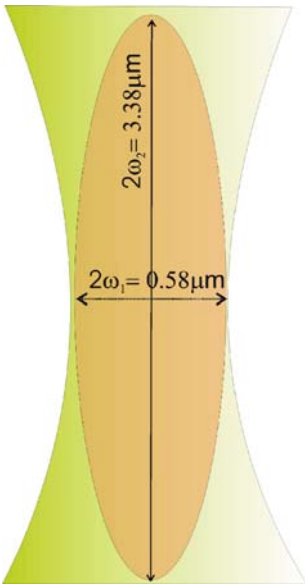

Fig. 1 Illustration showing a confocal volume in FCS (typical volume is around 1×10^{-15} l) enabling single molecule sensitivity. The dimension of the volume element was determined by using standard fluorophores (Rhodamine-6G and Alexa Fluor 488)

fusion coefficients, brightness, photophysical parameters, chemical equilibria etc.

FCS analysis fluctuations in the fluorescence signal over time arise mainly from diffusion of fluorescent species in and out of the detection volume. This small volume improves the signal-to-noise ratio and thus enables single-molecule sensitivity. The highly focused laser beam creates a diffraction-limited Gaussian–Lorentzian intensity profile with minimum lateral radius $\omega_1 = 0.29 \pm 0.05$ μm. The detection in the axial dimension (ω_2) is limited by a pinhole in the image plane of the microscope and was found to be $\omega_2 = 1.69 \pm 0.02$ μm. The size of the detection volume is 0.9 ± 0.1 fl.

The dimensions of the volume element were determined by using the standard fluorophores Rhodamine-6G and Alexa Fluor 488, given the standard diffusion coefficient (D) at 25 °C of both dyes is 2.8×10^{-10} m^2/s. Molecules diffuse through this illuminated volume over time, and give out photons which are recorded by the detection unit. Fluctuations in the detected fluorescence intensity are analysed by means of the autocorrelation function $G(\tau)$. To obtain real physical parameters from $G(\tau)$, one needs to apply a proper physical model. At this step first approximations take place. The detection volume is for bulk measurements approximated as a 3D Gaussian. Assuming small point-like non-interacting molecules freely diffusing in a space much larger than the detection volume, showing only the triplet state, the $G(\tau)$ takes

the form:

$$G(\tau) = 1 + \left(1 - T + Te^{-\tau/\tau_{tr}}\right) \left(\frac{1}{PN(1-T)}\right) \frac{1}{1+\left(\tau/\tau_D\right)} \left(\frac{1}{1+\left(\tau/\tau_D\right)\left(\omega_1/\omega_2\right)^2}\right)^{1/2}, \quad (1)$$

where T is the triplet fraction, τ_{tr} is the triplet decay time, PN is the apparent particle number, τ_D is the diffusion time, and ω_1 and ω_2 are the lateral and axial radii of the detection volumes. The derivation of equations for the applied models makes use of the natural laws applied in classical methods of perturbation kinetics, as the only difference is in the source of fluctuations.

The parameters PN and τ_D are related to macroscopic values of concentration c and diffusion coefficient D via:

$$\tau_D = \frac{\omega_1^2}{4D}, \quad (2)$$

and

$$PN = \pi c \omega_1^2. \quad (3)$$

The diffusion coefficient for spherically symmetric molecules is related to the hydrodynamic radius r_h via the Einstein–Stokes equation:

$$D = \frac{k_B T_C}{6\pi\eta r_h}, \quad (4)$$

where k_B is the Boltzmann constant, T_C is the thermodynamic temperature and η is the dynamic viscosity. The hydrodynamic radius r_h can be calculated from the molecular mass M using:

$$r_h = \sqrt[3]{\frac{3M}{4\pi\rho N_A}}, \quad (5)$$

where ρ is the mean density of the molecule and N_A is Avogadro's number.

The translational diffusion coefficient (D) depends largely on the shape of the molecule. For rod-like molecules, such as DNA, D can be estimated as:

$$D = \frac{Ak_B T_C}{3\pi\eta L}, \quad (6)$$

where L corresponds to the length of the rod (for DNA it is the rise per base pair (0.34 nm) multiplied by the number of base pairs), d is the diameter of the rod (2.38 nm for DNA) and A represents a correction factor:

$$A = \ln(L/d) + 0.312 + 0.565/(L/d) - 0.1/(L/d)^2. \quad (7)$$

It means that the diffusion coefficient of a 1000-bp DNA is approximately five times smaller and thus the diffusion time five times larger fora rod-like molecule than a spherical one. The DNA diffusion coefficient decreased by

increasing the DNA size, indicating the complex hydrodynamic properties of DNA with respect to translational diffusion [16, 17].

3 Simultaneous Lifetime and FCS Data Acquisition

The present state of the art in lasers, optics, photon detection and signal processing units enables many different single-molecule sensitivity set-ups. We applied an upgraded ConfoCor 1 fluorescence microscope to our NVGT research [18]. The basis is an inverted confocal epifluorescence microscope Axiovert 100. A pulsed picosecond 470-nm diode laser is coupled via an optical fibre to the back port of the microscope. Excitation light is reflected at a dichroic mirror to an overfilled water immersion objective, which focuses the light into a diffraction-limited spot (radius 250 nm). Emitted light is collected through the same objective, passes the dichroic mirror, is spatially filtered using a pinhole, and is detected by fast APD. Photon detection events are counted by a MicroTime 200 PCI board using the time-tagged

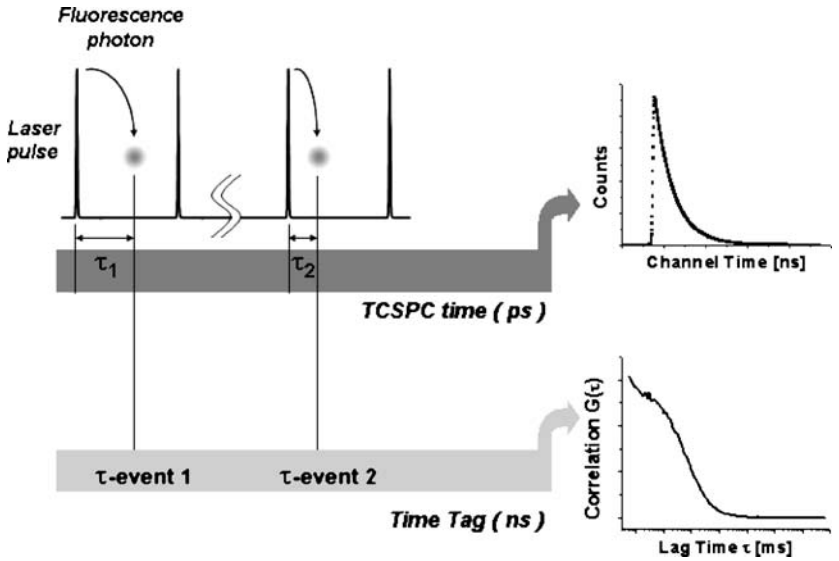

Fig. 2 The TTTR data acquisition mode enables monitoring of the full arrival kinetics of individual photons. The time tag (100 ns resolution) tells us the arrival time of the photon from the beginning of the experiment, and this information is used for calculation of the intensity trace and autocorrelation function $G(\tau)$. Time resolved means a time difference (40 ps resolution) between the laser pulse and detection of the photon. From this the fluorescence lifetime decay histogram is constructed. This simultaneous FCS and lifetime measurement helps to give more detailed information about the sample

time-resolved (TTTR) mode and saved to hard disk for further offline analysis.

The TTTR mode is advanced time-correlated single photon counting (TCSPC). In classical TCSPC, photon arrival times after the excitation (laser pulse) are measured and displayed as histograms. In TTTR mode, one measures and saves not only the time between excitation and emission (40 ps resolution), but also the arrival time from the beginning of the experiment (100 ns resolution), detector number (useless in a one-detector set-up) and sample position (again useless for a fixed set-up) (Fig. 2). Information-rich TTTR data can be analysed in many ways. We applied fluorescence lifetime determination from TCSPC times and FCS analysis of intensity fluctuations. The major advantages of this approach are that from a single measurement we simultaneously obtain information about the molecule microenvironment (carried in the fluorescence lifetime) and its diffusion properties, concentration and brightness (carried in the intensity fluctuations). Thus, we can directly correlate changes in one parameter with another.

4 Dyes for Efficient DNA Labelling

The study of DNA intercalation with EthBr was first reported by Webb's research group [19, 20], using the FCS technique. The DNA binding constant of EthBr and the DNA diffusion coefficient were reported using FCS. Kral et al. [21, 22] recently studied DNA condensation by using EthBr and propidium iodide (PI) in FCS. The count rate (CR), diffusion time (τ_D), and particle number (PN) observed by FCS at the single-molecule level, and their correlations, can be used to differentiate the nature of DNA/oligonucleotide–polycation interactions [21–25].

Although EthBr is a commonly used dye in DNA condensation studies, it was found to have effects on DNA structure at high concentrations. The helical axis of DNA was dislocated + 1.0 Å and the helix was twisted by 10°, giving rise to an angular unwinding of –26°, and the intercalated base pairs were tilted relative to one another by 8° [26]. Manning's theory of counterion condensation of polyelectrolytes [27] suggested that EthBr intercalation lengthens the DNA by about 0.27 nm [28]. This possible DNA conformation alteration is generally not a concern in steady-state fluorescence spectroscopy with a larger population to be measured, but this is detectable within the sensitivity of FCS. Additionally, the higher rate of EthBr release from DNA may also lead to a significant reduction in fluorescence, making fluorescence analysis more complex. This in turn leads to the search for new fluorescent dyes that can be used without significant change in DNA conformation and also possess high extinction coefficients (which allow them to be used at low concentrations), to avoid interference in the DNA condensation behaviour mediated by NVGT vectors.

Recently, a new unsymmetrical monomethine cyanine dye, PicoGreen® (PG) (Fig. 3), was introduced as a patented fluorescent dye from Roth, Haughland and co-workers at Molecular Probes [29, 30]. Its chemical structure was recently reported by Vitzthum and co-workers, confirmed by NMR and MS techniques and named as [2-[*N*-bis(3-dimethylaminopropyl)amino]-4-[2,3-dihydro-3-methyl-(benzo-1,3-thiazol-2-yl)-methylidene]-1-phenyl-quinolinium]$^{+}$ (Fig. 3a) [31]. However, this name could also be (Chem Abs 9th CI): 2-[bis(3-dimethylaminopropyl)amino]-4-(3-methyl-2(3*H*)-benzothiazolylidene)methyl-1-phenyl-quinolinium [32] [178918-98-4] and/or 2-[bis(3-dimethylaminopropyl)amino]-1-phenyl-4(1*H*)-quinolinylidene)methyl)-3-methyl-benzothiazolium [33] [771577-99-2]. The charge due to quaternization of the aromatic N atoms is delocalized, probably equally well shown residing on the *N*-methyl-benzothiazolium (Fig. 3a) [33] and on the *N*-phenyl-quinolinium (Fig. 3b) [32], in a solvent- and environment-dependent manner. There is also a contribution from the third mesomer, including the lone-pair electrons on the anilino tertiary amine, as its ammonium ion (Fig. 3c) [34].

From DNA intercalation structure–activity relationship considerations, PG carries three positive charges, i.e. one on nitrogen in the conjugated, mesomeric, heteroaromatic system and two at the 3-dimethylaminopropyl residues. The cationic side chain of PG (compared to EthBr) contributes to

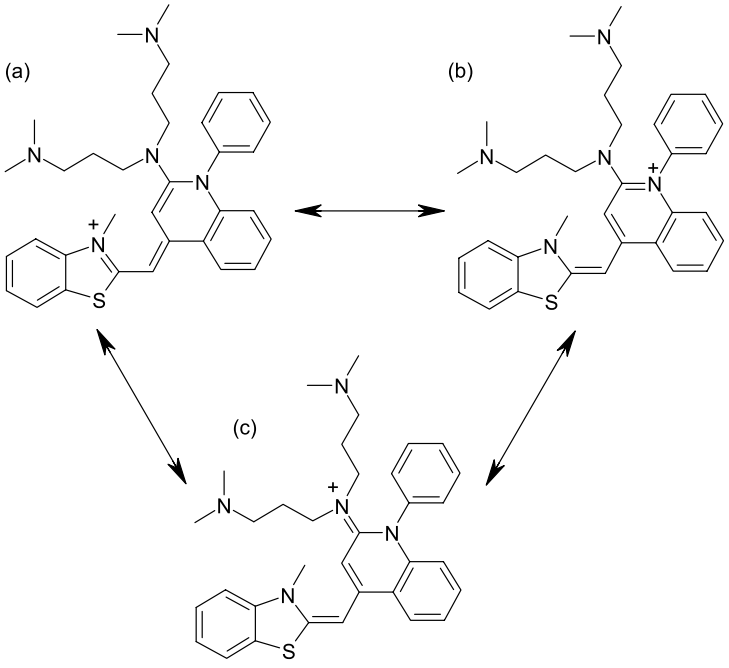

Fig. 3 PicoGreen® (PG), an unsymmetrical monomethine cyanine dye containing a polyamine side chain to improve DNA-binding affinity with three mesomers (**a**, **b** and **c**)

higher affinity for double-stranded DNA (dsDNA). Biphasic-mode binding was reported for PG interaction with dsDNA. Base-pair intercalation happens at a low dye/base pair ratio, and external binding (minor groove) was found at a higher dye/base pair ratio. At low dye/base pair ratio, PG shows no base sequence specificity. However, the fluorescence intensities of PG–DNA complexes were related to the DNA sequence at higher ratios. The increase in fluorescence intensity of PG upon binding to DNA is about 1000-fold (extinction coefficient 70 000 M^{-1} cm^{-1}) and this makes the background fluorescence from free dye negligible. A small red shift of the peak absorption (from 498 nm for free dye to 500 nm for the bound dye) was observed for PG [35]. Re-equilibration can be reached in seconds upon PG labelling on dsDNA. These favourable kinetics also make PG one of the most efficient and versatile DNA probes [36]. Interestingly, PG binds selectively to single-stranded DNA (ssDNA) (low affinity) and dsDNA (high affinity) at 525 nm, unlike EthBr at 610 nm. Thus, the use of PG with EthBr simultaneously at dual wavelength (525 and 610 nm) was recently established as a novel efficient tool to determine the DNA unwinding condition (ss:dsDNA ratio) [37, 38]. The low affinity of PG for ssDNA helps to ensure that fluorescence detection mainly arises from dsDNA–PG interactions.

In NVGT research, PG was used to determine the quantity of free DNA (uncomplexed DNA) to assess the DNA condensation property of gene vectors [39–42]. Currently, there is no study using low-concentration PG to assess complexed DNA during DNA condensation.

5
Calf Thymus DNA Classical FCS Studies

5.1
Calf Thymus DNA–PicoGreen Interaction Study

Calf thymus DNA (ct DNA) is a linear DNA with minimum kilobase pairs (kbp) = 13 (MW 8580 MDa). Also, as calculated from: $L = N_{DNA} \times a$, given N_{DNA} is the average number of DNA monomers (base pair) and a = monomer length (i.e. 0.34 nm rise per base pair for DNA duplex), its contour length is 4.4 μm. PG was used in our study to monitor ct DNA. In comparison with EthBr, PG intercalation affinity to dsDNA is higher, and it also has a higher absorption extinction coefficient. PG labels nucleic acid uniformly and without any concentration dependence or artefacts [43]. Free PG also has no significant fluorescence unless intercalated, thus background fluorescence is negligible. In our experiments, fluorescence fluctuation was observed and recorded over the increase of PG concentration (i.e. labelling ratio). Experimental $G(\tau)$ functions were satisfactorily fitted to a theoretical diffusion model with a single fluorescent type. Typical normalized autocorrelation functions $G(\tau)$ are plotted as shown in Fig. 4.

When ct DNA is labelled with PG the diffusion time remains constant throughout the whole dye concentration range, showing that the plasmid conformation is not altered by the dye association (Fig. 5). The fluorescence intensity per plasmid particle rises monotonically. The apparent PN saturates at ten dye molecules per 1 kbp of the ct DNA. PN calculated from $G(\tau)$ of PG molecules bound to ct DNA was 43.1 ± 8.1. This may be explained from the DNA length, as ct DNA (contour length = 4.4 μm) is considerably bigger than the confocal element ($\omega_1 = 0.58$ μm, $\omega_2 = 3.4$ μm). In a recent paper [44], it was proposed that long DNA may have internal conformation diffusion of its chain (segmental motion). This leads to a high number of fluctuations in the fluorescence intensity, i.e. lower $G(\tau)$, especially when considering that the laser focus could excite at least one part of the entire chain, and thus finally to a higher PN.

Furthermore, at concentrations where apparent PN stabilizes the fluorescence intensity, "count rate" (Fig. 5) is still rising thus indicating that all particles are labelled only after a certain amount of dye is added. Further increase of the fluorophore quantity makes only the fluorescence intensity rise. These results show that the ideal dye/DNA ratio should give a sufficient fluorescence signal with less interference in DNA conformation from intercalating

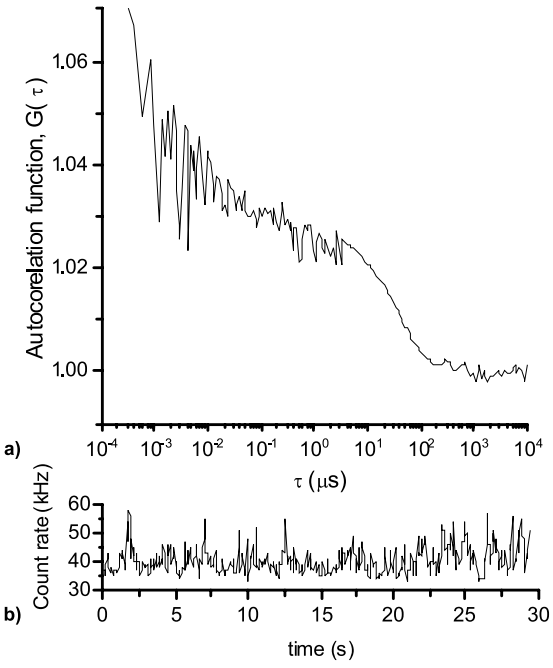

Fig. 4 Examples of normalized autocorrelation functions $G(\tau)$ (**a**) and the relative count rates (**b**) for ct DNA (1 nM, 200 μl) intercalated with PG (1.1×10^{-6} M, 30 μl); C_{dye}/C_{kbp} is 13. The nature of multi-labelling DNA (long-chain molecules) causes an overestimation of PN (apparent PN) compared to the PN of singly labelled small molecules

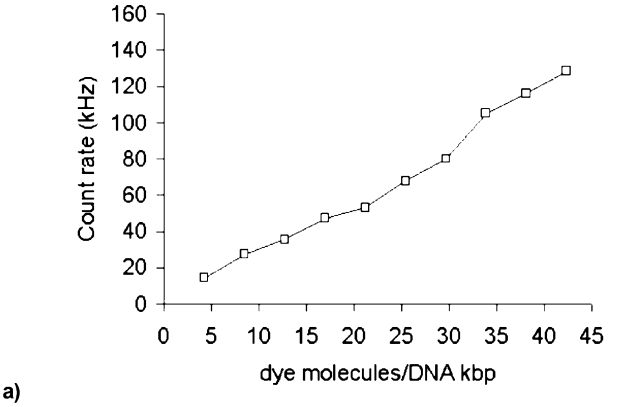

a)

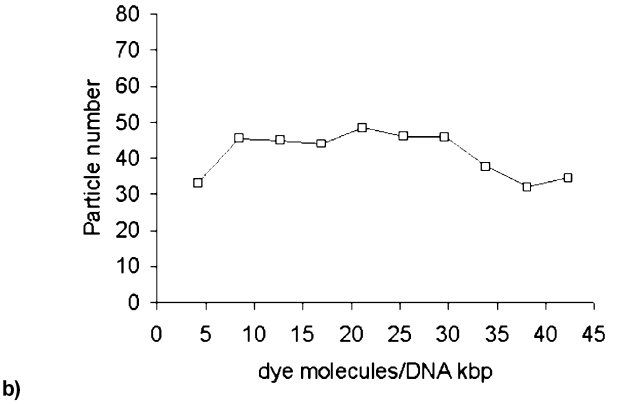

b)

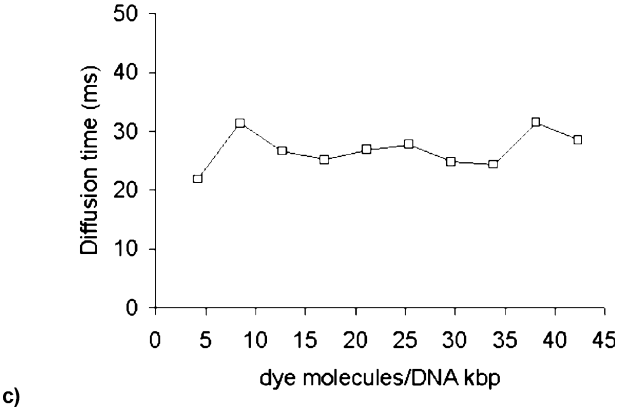

c)

Fig. 5 PG labelling calibration using ct DNA. Different volumes of PG (1.1 μM) were added to 200 μl of 1 nM DNA and incubated for 10 min. $G(\tau)$ was recorded at each dye labelling ratio. FCS parameters were calculated and plotted against dye concentration, i.e. **a** count rate (CR), **b** particle number (PN) and **c** diffusion time (τ_D)

dyes. This suggests that PG has no influence over the hydrodynamic properties of DNA molecules. Additionally, PG can be used at a very low level (i.e. 5–40 dye molecules/kbp) compared to the similar study using EthBr [21, 22, 24]. The stability of the dye and DNA complexes after dilution is also important for a titration study of DNA condensation. The high stability of PG-labelled DNA samples means that the volume addition of DNA condensing agent does not affect the accuracy of the measurement [35].

The diffusion coefficient of ct DNA was calculated by considering DNA as a rod-like molecule [21, 22, 24]. Considering the characteristics of DNAs, ct DNA has a high τ_D which is due to its significantly greater size than circular plasmids; different length DNAs diffuse differently in solution. The D of ct DNA from calculation (5.3×10^{-13} m^2/s) shows a similar result to that found in FCS experiments (7×10^{-13} m^2/s). The deviation of τ_D found in our FCS studies and from calculation was noticeably high for ct DNA, which may suggest that the long DNA may diffuse differently from the shorter one with some additional mechanism. The other contribution factor is also from the polydispersity of ct DNA, which means that a different length of linear DNA was measured at once. However, the DNA condensation process is regarded as an all-or-nothing process; it is possible to monitor nanoparticle formation using ct DNA [45, 46].

5.2 Calf Thymus DNA Condensation by Lipopolyamines

Lipopolyamine vectors have been regarded as efficient DNA condensing agents in NVGT. These molecules have a lipophilic moiety (mainly long chain hydrocarbon or steroidal lipids) and positively charged amine group(s), such as spermine or synthetic polyamines [47–52]. Two lipopolyamines were synthesized and used in these experiments. Both are designed to incorporate a spermine backbone conjugated with a lipophilic moiety, i.e. the oleoyl group (amide link) (Fig. 6a) [47, 49, 50] and the cholesteryl group (carbamate link) (Fig. 6b) [52]. Both our novel DNA condensing agents show effective condensation (i.e. yielding 10% fluorescence reduction in a fluorometric assay at ammonium/phosphate (N/P) ratio as low as 1.5–2.0) and high transfection rate. One aim of this study is to understand more on the mechanism of how these two vectors interact with DNA at a single-molecule level (in this case, specifically regarded as a single nanoparticle) by FCS using PG.

From the calibration curves (Fig. 5a–c), the optimal dye ratio used for ct DNA labelling was in the range of 5–40. PG was prepared in 1 : 200 dilution (according to the manufacturer's protocol). In the DNA condensation experiment, the PG volume added was 30 μl (which is equivalent to a dye/kbp ratio = 35). Fluorescence fluctuation was monitored while adding N^4,N^9-dioleoylspermine or N^1-cholesteryl spermine carbamate in a solution sample containing PG-labelled DNA.

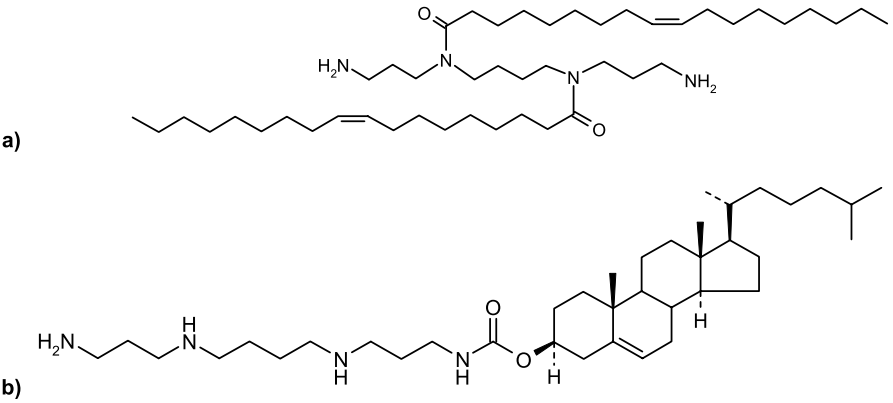

Fig. 6 **a** N^4,N^9-Dioleoylspermine, **b** N^1-cholesteryl spermine carbamate. The aim of this study is to understand more of the mechanisms by which these two vectors interact with DNA at a single molecule level (in this case, specifically regarded as a single nanoparticle) by FCS using PG

When the N/P ratio was increased (Fig. 7), DNA phosphate groups were gradually neutralized by positively charged ammonium groups of N^4,N^9-dioleoylspermine and N^1-cholesteryl spermine carbamate. $G(\tau)$ was recorded and FCS parameters (diffusion coefficient and PN) were then calculated throughout the DNA condensation process. The indication of DNA condensation occurrence is the dramatic decrease of τ_D and PN, particularly for a system with macromolecules where a single monitored molecule is not small enough to fit in the confocal volume. From Fig. 7, the diffusion coefficient (D) continuously increased upon the addition of lipopolyamines in both DNA condensation experiments. As faster movement of DNA resulted from condensation, we conclude that smaller (compacted) DNA nanoparticles have been formed. The PN also decreased while measured CR remained constant.

5.3
Point-like Molecule Detection in DNA Condensation

PN is a direct parameter to prove the number of fluorescent molecules, which here reports on the DNA concentration. In the model with point-like molecules, PN is described by the equation $\mathrm{PN} = C \times V \times N_A$, where C = molarity of detected molecules, V = confocal volume, and $N_A = 6.023 \times 10^{23}$. By using this equation, and as the DNA concentrations used in our experiments were kept constant at 1 nM, the theoretical PN to be achieved is around 1. The PN achieved at N/P = 1.0–1.5 for ct DNA condensed by N^4,N^9-dioleoylspermine was 0.7. This evidence confirms that DNA was condensed into a point-like molecule by the C_{18}-substituted lipopolyamine, which fulfils the assumptions of FCS and validates the use of FCS as a sensitive method in DNA formula-

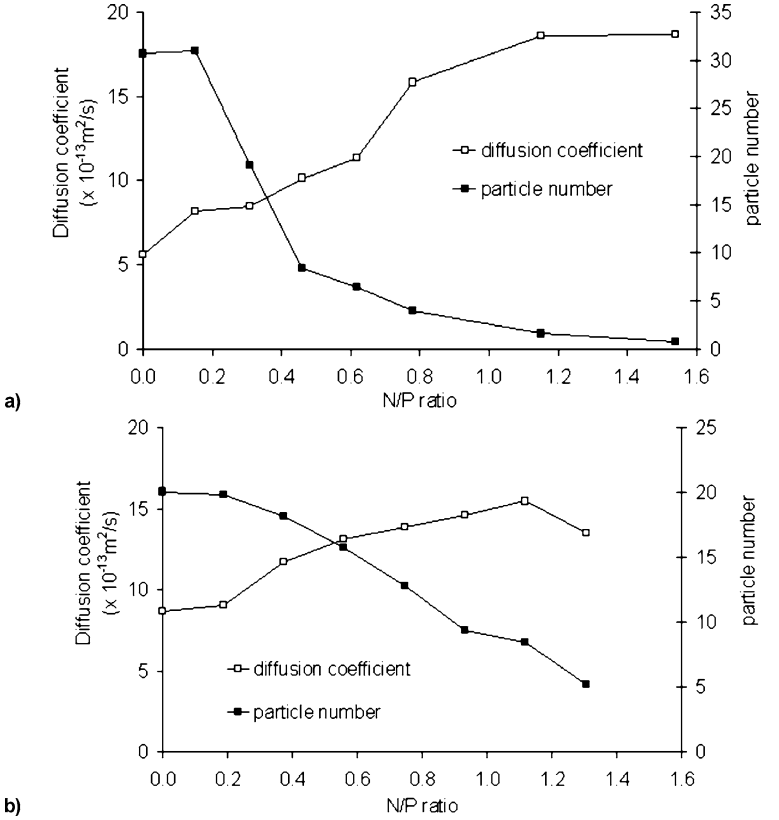

Fig. 7 FCS study of DNA nanoparticle formation: ct DNA (1 nM, 200 μl) was condensed with lipopolyamines, using PG as a reporter probe. **a** ct DNA condensation by N^4,N^9-dioleoylspermine (PG at dye/kbp = 13), **b** ct DNA condensation by N^1-cholesteryl spermine carbamate (PG at dye/kbp = 13)

tion studies (which is indeed a point-like molecule, when compared to the typical confocal volume). This result is in agreement with other physical studies on DNA particle size, when completely condensed at the nanoscale level. Similar results were also found for DNA condensation with N^1-cholesteryl spermine carbamate, with a decrease in τ_D and PN. The PN value achieved at N/P = 1.5–2.5 for ct DNA condensed by N^1-cholesteryl spermine carbamate was 5.2. From a comparison of this PN result with that obtained with N^4,N^9-dioleoylspermine, we conclude that N^1-cholesteryl spermine carbamate is a poorer DNA condensing agent than N^4,N^9-dioleoylspermine. Additionally, the condensation occurred at a higher N/P ratio (N/P = 1.5–2.5) than the condensation achieved with N^4,N^9-dioleoylspermine (N/P = 1.0–1.5). Considering the positive-charge number of N^4,N^9-dioleoylspermine is less than that of N^1-cholesteryl spermine carbamate (i.e. 2 compared to 2.4), we conclude that

the more efficient DNA condensation is possibly due to the respective regiochemical distribution of these two positive charges together with their lipid moieties (C_{18} vs cholesterol).

Point-like molecules obtained from ct DNA condensation by N^4,N^9-dioleoylspermine have an average τ_D of 12.0 ms ($D = 1.8 \times 10^{-12}$ m^2/s). These nanoparticles diffuse about three times faster than free DNA ($D = 0.71 \times 10^{-12}$ m^2/s). A similar diffusion behaviour of ct DNA complexed with N^1-cholesteryl spermine carbamate was also found at 14.0 ms ($D = 1.3 \times 10^{-12}$ m^2/s), although the PN has not fulfilled the point-like molecules hypothesis (i.e. not approximating to 1.0). The change in the magnitude of the diffusion coefficient (D) between free and condensed DNA, mediated by both our two lipopolyamines and at appropriate N/P ratios to achieve full DNA condensation, provides evidence for the dramatic change that is DNA condensation. Moreover, D is, in general for point-like molecules, a rather insensitive parameter and could incorporate some error (about 10%). On the other hand, PN is much more sensitive, and it accurately shows differences between both condensing agents. Thus, N^4,N^9-dioleoylspermine is a more efficient DNA condensing agent (PN approaching 1.0) than N^1-cholesteryl spermine carbamate.

In the steady-state EthBr fluorescence quenching study, it was shown that there is no significant difference in the condensation of ct DNA and plasmids. However, FCS is a single-molecule technique with high sensitivity, and it is possible to observe the difference of linear (and big) ct DNA behaviour and plasmid (circular) DNA in a 1-fl confocal volume.

6
Simultaneous Lifetime and FCS Studies of Plasmid DNA

Titration experiments of chromophore–DNA complexes using classical FCS yield information about changes in diffusion behaviour (caused by conformational changes) during condensation. These changes can be accompanied by changes in dye environment, which can be reflected in fluorescence lifetime change. Therefore, in our study, we have applied simultaneous lifetime and FCS analysis [18] to monitor the behaviour of PG on plasmid DNA at low labelling ratio (40 dye/kbp) through its condensation process. The set-up used (pulsed laser and TTTR data storage) allows the simultaneous monitoring of DNA condensation (through FCS analysis) and PG lifetime (through the time-resolved mode).

6.1
Plasmid DNA–PicoGreen Labelling Study

pGL3 DNA (5.3 kbp, contour length 1.8 μm) and pEGFP (4.7 kbp, contour length 1.6 μm) are two circular plasmids used in simultaneous lifetime and FCS

experiments. It was expected that the smaller size of both plasmids (compared to linear ct DNA) would result in a higher diffusion coefficient and smaller PN when they are detected using FCS and PG.

pGL3 and pEGFP were prepared in HEPES buffer (20 mM NaCl, pH 7.4) in 1 nM concentration and used in 200 μl volumes. Increasing amounts of PG (as a 1.1 μM solution) were added to both plasmids to perform a measurement simulating the different states of PG binding. Experimental $G(\tau)$ functions were satisfactorily fitted to a theoretical diffusion model with two-population fluorescent types, which show (more than 95%) a major population of a slow diffusing species. Typical normalized autocorrelation functions $G(\tau)$ are shown in Fig. 8.

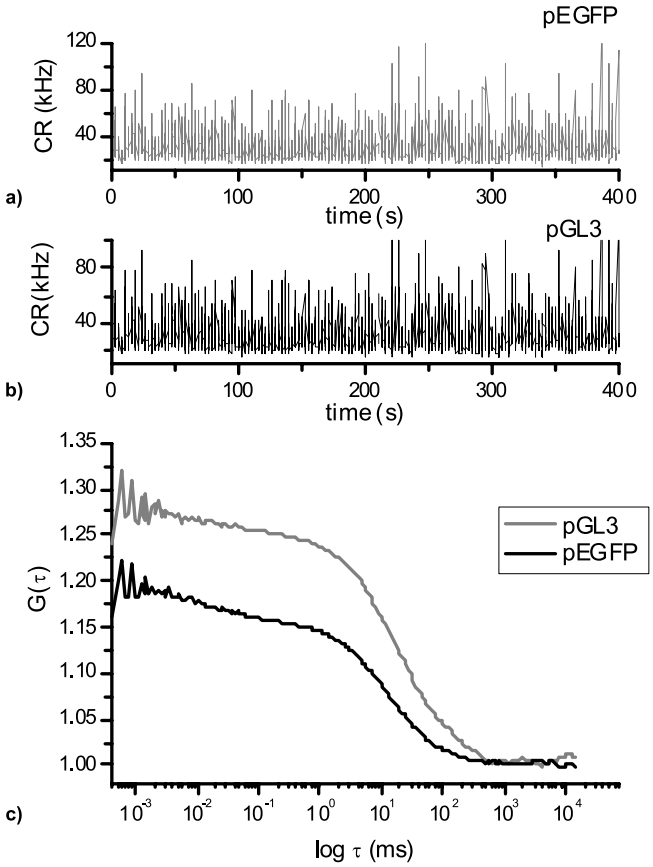

Fig. 8 Examples of CR plots and normalized $G(\tau)$ constructed from TTTR data. The CR tracking (**a** pEGFP, **b** pGL3) and $G(\tau)$ (**c**) for pGL3 (1 nM, 200 μl) intercalated with PG (1.1 μM, 18 μl) (*black line*) and pEGFP (1 nM, 200 μl) intercalated with PG (1.1 μM, 18 μl) (*grey line*); C_{dye}/C_{kbp} are 18 and 21, respectively. The nature of multi-labelling DNA (long-chain molecules) causes an overestimation of PN (apparent PN)

According to the $G(\tau)$ obtained from TTTR data analysis, both PG-labelled plasmids show similarity in their autocorrelation functions (Fig. 8). These similar diffusion coefficients correspond to the similar size and structure of pGL3 and pEGFP. Both DNAs also show the overestimated PN, higher than the theoretical PN (calculated by the real concentration of DNA used) as previously discussed for ct DNA. This is caused by the size of multi-labelled plasmid DNA, which is too big to fit the confocal volume. This leads to a multiplicity of observed PG on a single DNA molecule.

The FCS parameters (Fig. 9), calculated from $G(\tau)$ and the confocal volume obtained from Alexa Fluor 488 calibration, are complementary to the lifetime

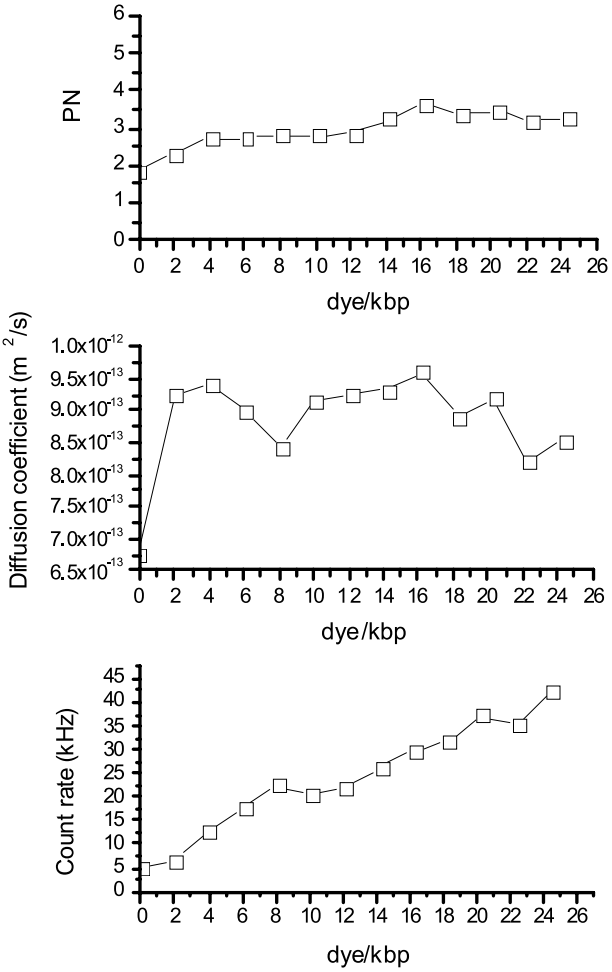

Fig. 9 FCS parameters from TTTR data acquisition, i.e. PN, CR and diffusion time (or coefficient), of PG-labelled pGL3 (□) were analysed from $G(\tau)$. PG was added to DNA solutions achieve different dye/kbp ratios

information of fluorescent PG. The constant increase of CR when more PG was added confirmed that PG intercalation is the most preferable binding mode in the low-labelling condition (less than 40 kbp). This is important to DNA probe selection which the unity of binding mode may simplify for data interpretation. The constant PN at a value of 3–5 and diffusion coefficient (1×10^{-12} m^2/s) suggest that DNA-bound PG molecules do not alter the DNA hydrodynamic property (i.e. do not induce DNA bending or even condensation).

In Fig. 10, the PN and diffusion coefficient (1.5×10^{-12} m^2/s) of labelled pEGFP were similar to those of pGL3 (1×10^{-12} m^2/s). However, the PN of PG-labelled pEGFP was slightly increased and finally attained a constant level.

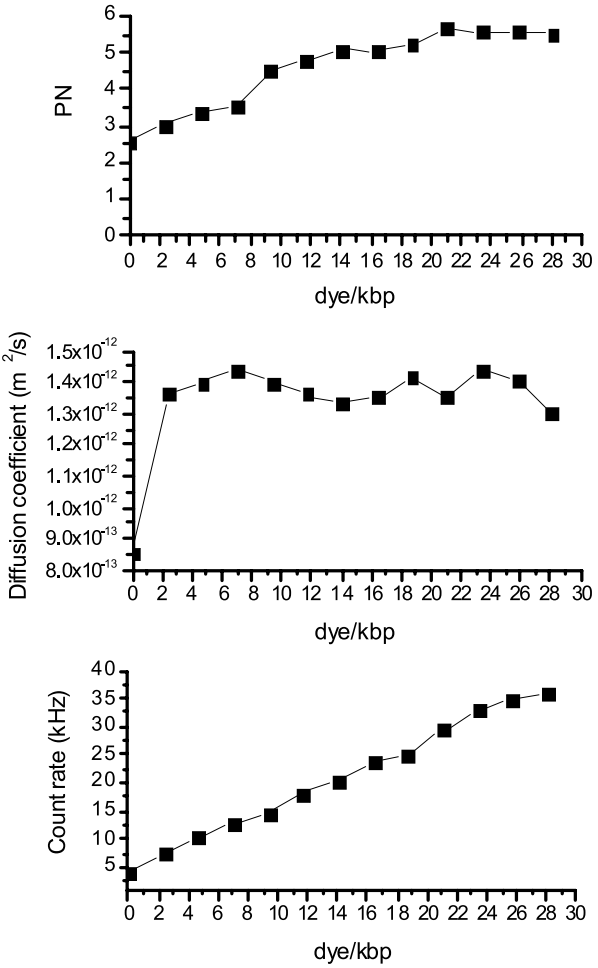

Fig. 10 FCS parameters from TTTR data acquisition, i.e. PN, CR and diffusion time (or coefficient), of PG-labelled pEGFP (■) were analysed from $G(\tau)$. PG was added to DNA solutionsto achieve different dye/kbp ratios

This increased PN may result from the DNA labelling distribution of PG, where initially PG molecules are localized at preferential binding sites on DNA (apparent lower PN), then PG molecules are randomly distributed over the DNA double helical chain, so the apparent PN becomes slightly higher, and finally, PN reaches its constant value. However, this possible DNA base-preference of PG binding was not found in pGL3. According to the literature [38], PG also shows higher affinity to GC than AT. This slight increase of PN does not affect PG fluorescence in DNA when it is used to monitor the DNA condensation process.

To understand the nature of DNA inding of PG, fluorescence TTTR data were recorded at different PG dye/kbp ratios using pGL3 and pEGFP. The

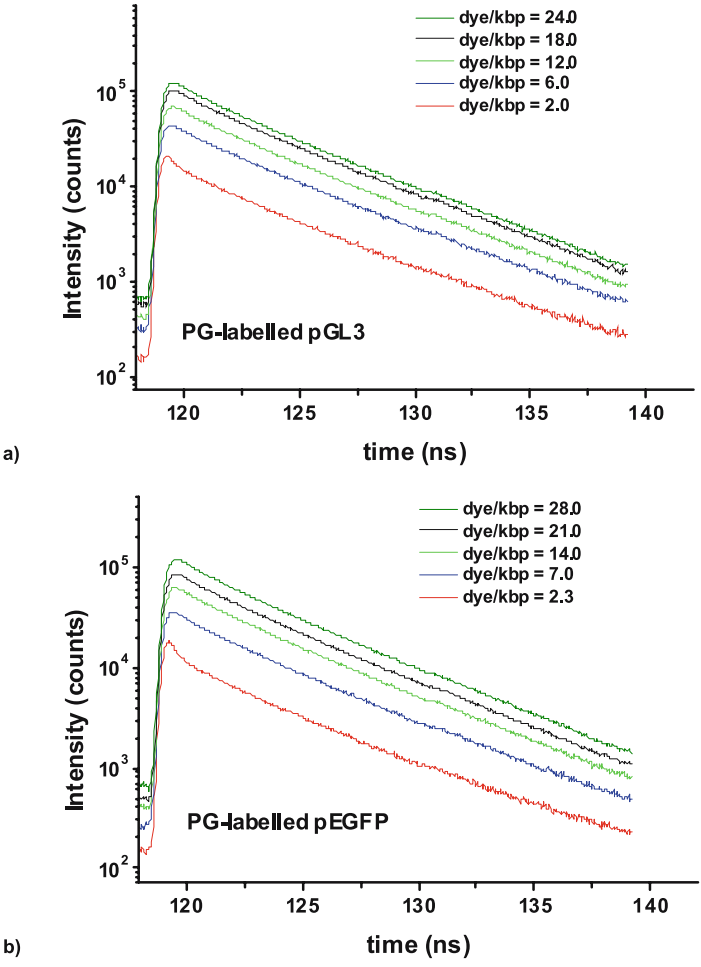

Fig. 11 Fluorescence decay profiles for PG bound to circular plasmid DNA (**a** pGL3 and **b** pEGFP) obtained from TTTR data acquisition

intensity decay was obtained from TTTR data and fitted by MicroTime 200 (Fig. 11 plotted in OriginPro 7.0). A tail fitting was used in this experiment at constant channels. PG-labelled DNA fluorescence lifetime decay was best fitted by a two-exponential model. From this fitting calculation, there are two populations of DNA-bound PG fluorescent species: (a) $\tau = 4$ ns (intensity fraction 97%) and (b) $\tau = 1$ ns. Considering that the fraction of other PG species (with $\tau = 1$ ns) is very small, we concluded that the $\tau = 4$ ns species is the major fluorescent PG (Fig. 12). This corresponds well to the previous study

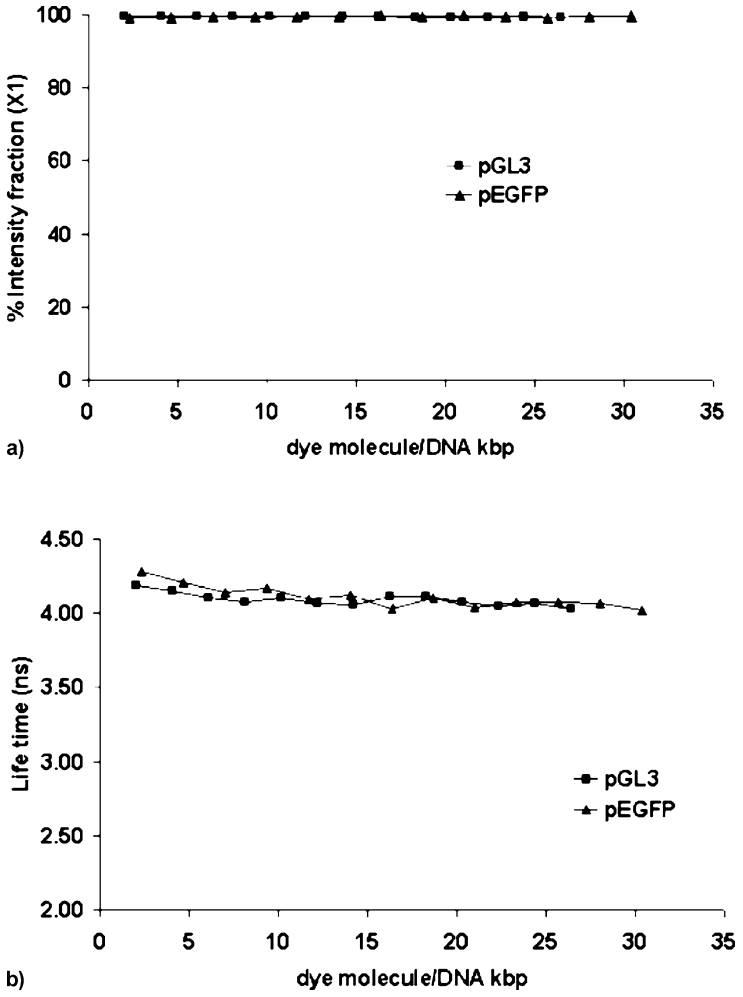

Fig. 12 **a** Major fraction of fluorescent species (97%) and **b** lifetime of the major fluorescent population over a range of dye labelling ratios. The major fluorescent species of DNA-bound PG shows a consistent lifetime, indicating that there is no dye relocation or dye environment change

by fluorescence lifetime measurement with a streak camera by Schweitzer and Scaiano [38], who also showed that PG is adequately fitted by mono-exponential decays when complexed to dsDNA (within ±5% error). In terms of model fitness, the two-exponential model has improved the χ^2 value over the mono-exponential model, but a three-exponential model failed to improve the χ^2 value further. Thus, we used the two-exponential model throughout our experiments.

Figure 12 reveals that the majority of PG, in the range of 0–30 dye molecules/kbp, is bound to both plasmid DNAs through a single and unified mechanism. PG-labelled DNAs show negative in the circular dichroism study [53], indicating that majority of dyes are intercalated between DNA base pairs. This is also supported by the PG concentration used in our study, which is much lower than the saturation of acridine dye intercalation (i.e. 500 dye molecules/kbp). However, our model also indicates the presence of short-lived PG (1 ns), though in very small numbers. The constant lifetime of DNA-bound PG at 4 ns also confirms that there is no change in the environment surrounding PG intercalating sites. This ensures that there is no major change in DNA conformation due to PG intercalation, which is a desirable property of a good fluorescent probe for DNA.

6.2 Simultaneous Lifetime and FCS Analysis of Plasmid DNA Through the Condensation Process

Two lipopolyamines, N^4,N^9-dioleoylspermine (Figs. 13 and 14) and N^1-cholesteryl spermine carbamate (Figs. 15 and 16), were used in this study to condense pGL3 and pEGFP. The FCS parameters were obtained from $G(\tau)$ (derived from TTTR data) and show efficient condensation of both plasmids.

DNA conformational change toward a condensed DNA was reflected in lower PN values with increased N/P charge ratios. More structured DNA would have less segmental movement, thus reducing the PN value. Based on our previous study, these two lipopolyamines can achieve the point-like molecule condition (DNA was seen as one nanoparticle), because the observed PN (= 1.0 for both plasmids) is approaching the theoretical PN = 0.6 (for 1 nM DNA). Complete DNA condensation was also illustrated by the increase of the diffusion coefficient (D) of fluorescently labelled plasmid.

PG lifetime data, additional information obtained from TTTR data, can be used to explain the behaviour of PG when DNA is condensed. The fluorescence decay profile of DNA-bound PG was fitted by employing the two-exponential model. The decay plots are shown in Figs. 17 and 18. The major population of fluorescent species in condensed DNA was also found to be 97% consistently through the condensation process, with lifetime at 4 ns, which is the same as previously noted in the experiments (without

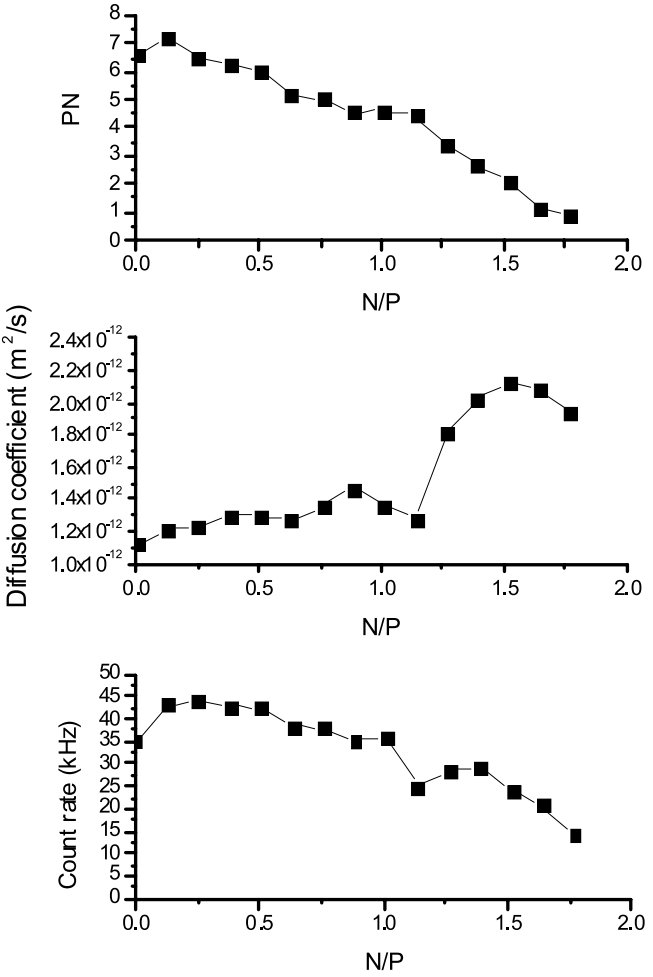

Fig. 13 FCS parameters derived from TTTR data acquisition during the condensation process of pGL3 by N^4,N^9-dioleoylspermine; PG used at 18 dye/kbp

lipopolyamines) shown in Fig. 12. This emphasized that most PG molecules remain in the same binding site and there was no migration to other binding sites (i.e. minor groove).

The lifetime values (Fig. 19b) found in our DNA experiments were decreased from 4 to 3.0–3.5 ns at the last stage of DNA condensation. We conclude that even though PG still maintains its binding sites, there might be some changes in the surrounding environment of the DNA base pairs, and this promotes fluorescence loss at a quicker rate (i.e. fluorescence quenching). This quenching was probably due to DNA packing into nanoparticles in the condensed DNA environment.

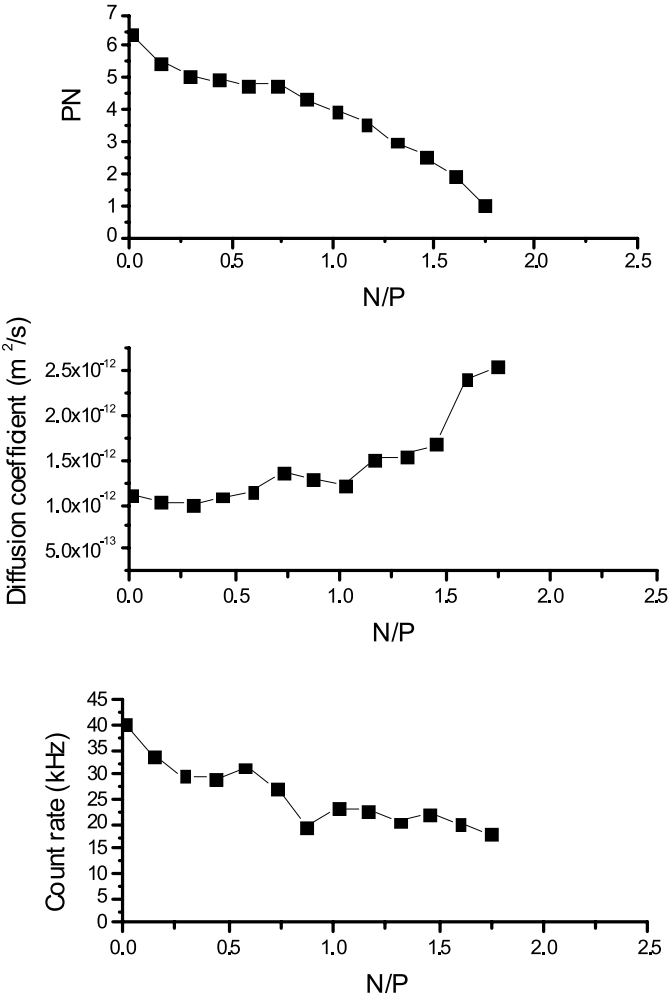

Fig. 14 FCS parameters derived from TTTR data acquisition during the condensation process of pEGFP by N^4,N^9-dioleoylspermine; PG used at 21 dye/kbp

Both CR and lifetime were normalized to the percentage of fluorescence decrease. This use of lifetime (time unit) as a fluorescence unit was based on the relationship of fluorescence quantum yield and lifetime, as described in the equation:

$$\frac{F_0}{F_q} = \frac{\tau_0}{\tau_q} . \tag{8}$$

The CR values were reported as % relative CR, which included both dye release (physical loss of dye from DNA) and dye quenching (no physical loss of

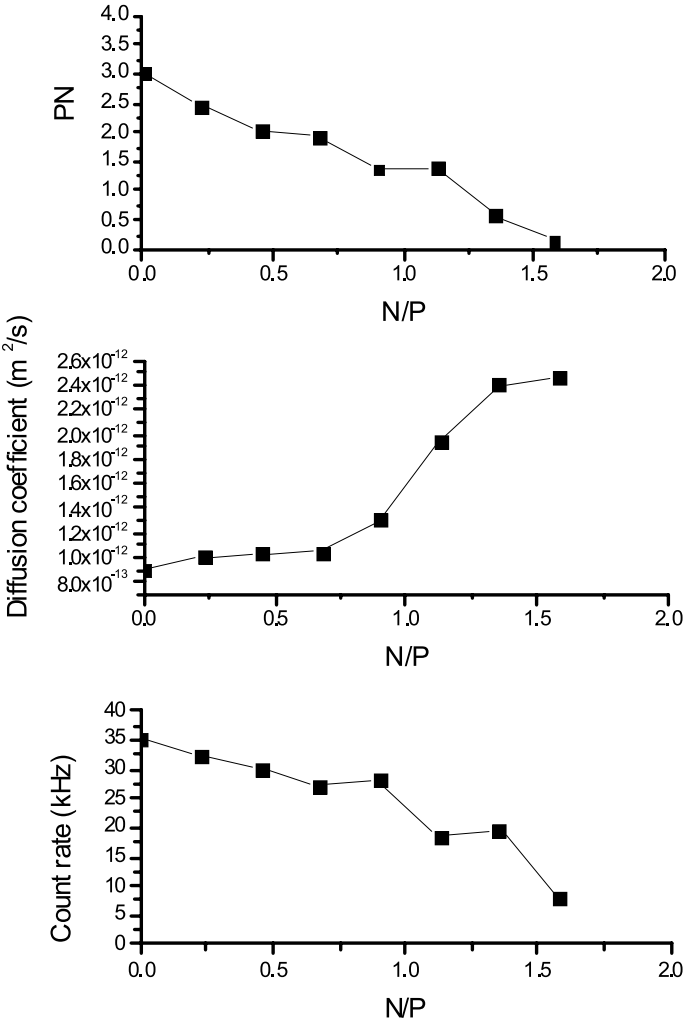

Fig. 15 FCS parameters derived from TTTR data acquisition during the condensation process of pGL3 by N^1-cholesteryl spermine carbamate; PG used at 18 dye/kbp

dye, but shorter lifetime). During the first stage of DNA condensation, only the dye release process leads to CR loss. The dye release process does not decrease the decay time of PG, because only the fluorescent species (intercalated PG) was monitored. This is supported by Figs. 20 and 21, in which lifetime is found to be constant during the dye release process. At the stage of nanoparticle formation, dynamic quenching of PG is proposed as the process leading to fluorescence loss. The quenching process acts on the excited population and thus decreases the mean decay time of the excited-state population.

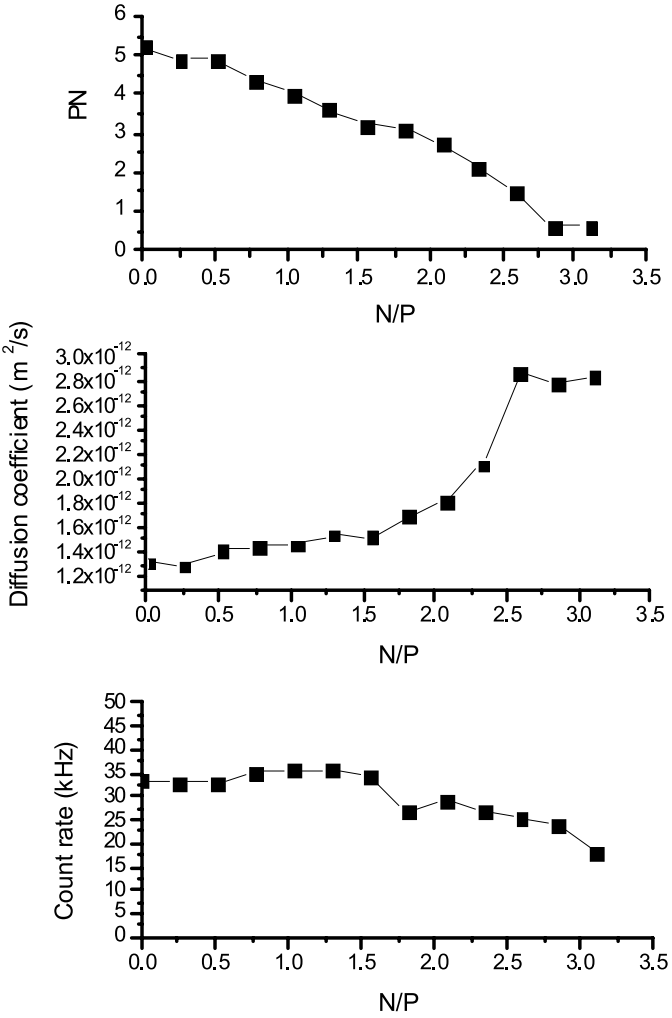

Fig. 16 FCS parameters derived from TTTR data acquisition during the condensation process of pEGFP by N^1-cholesteryl spermine carbamate; PG used at 21 dye/kbp

The behaviour of PG on DNA during condensation is shown in our model (Fig. 22). PG efficiently binds to DNA (step I dye binding) with a single binding mode (intercalation), a 4-ns lifetime, and no interference in DNA hydrodynamics. Upon adding the lipopolyamine DNA condensing agent to the DNA–PG complex, a small fraction of PG molecules were excluded from the complex. However, the degree of PG release also depends on the condensing agent used (step II dye release). This does not indicate the end point of DNA nanoparticle formation. On the addition of further lipopolyamine, the circular plasmid DNA was transformed into a single nanoparticle (step III dye quenching).

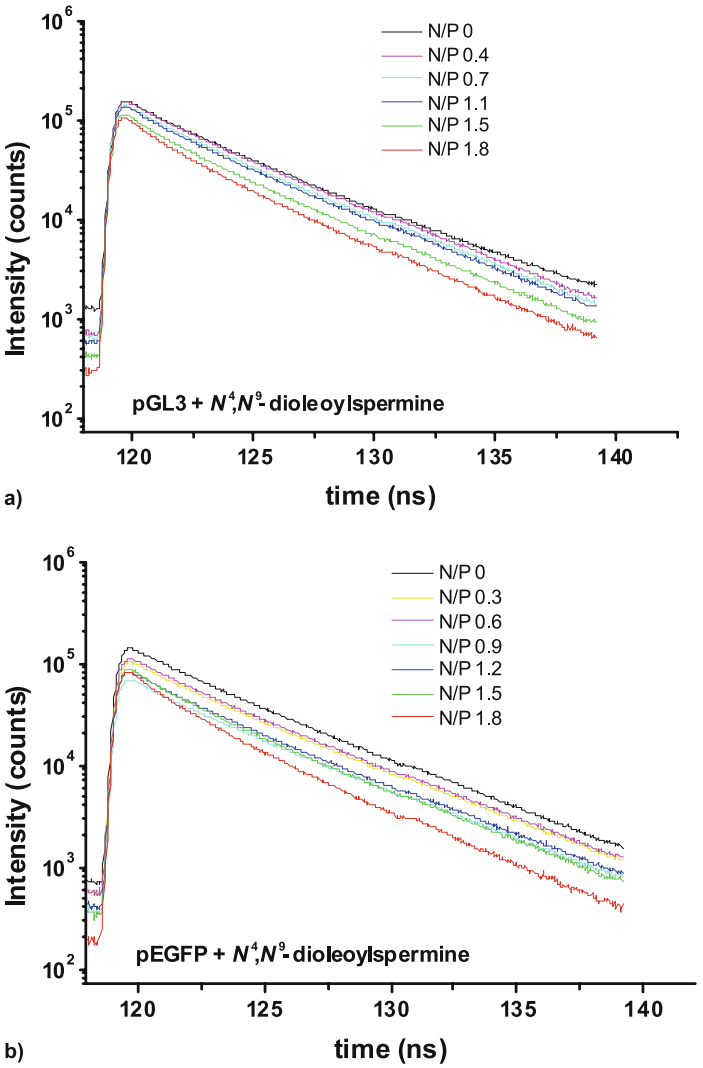

Fig. 17 Fluorescence decay profiles for PG bound to circular plasmid DNA (**a** pGL3 and **b** pEGFP), obtained from TTTR data acquisition, which undergoes DNA condensation using N^4,N^9-dioleoylspermine

Dye quenching, as determined by lifetime analysis, is an effective indicator of nanoparticle formation. In step III, the measured PN, a reliable parameter for FCS measurement, approached the theoretical PN. Key advantages in the use of PG in these DNA condensation studies are, at the low concentrations employed (essentially 100 nM), its single (97%) mode of binding to DNA (intercalation) and, in comparison with other dyes such as EthBr, its high affinity for DNA.

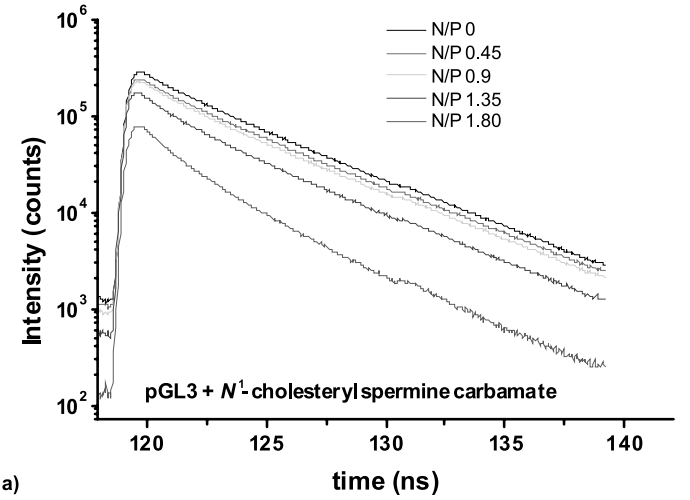

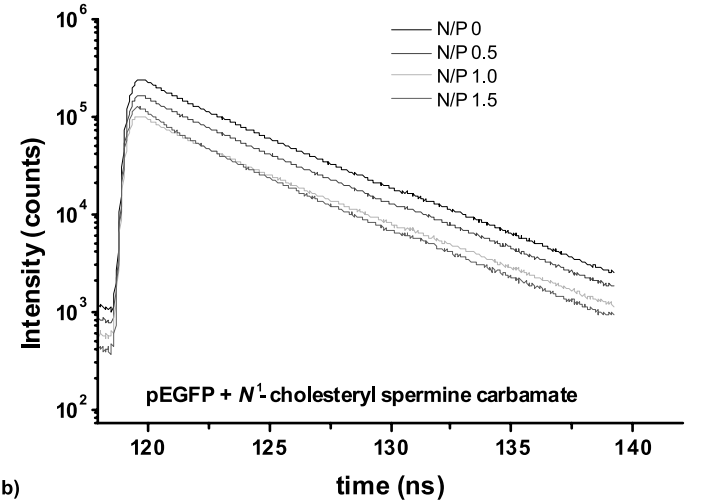

Fig. 18 Fluorescence decay profiles for PG bound to circular plasmid DNA (**a** pGL3 and **b** pEGFP), obtained from TTTR data acquisition, which undergoes DNA condensation using N^1-cholesteryl spermine carbamate

7 Conclusions

Employing the reported FCS experiments, we were able to monitor lipopolyamine–DNA complex formation at the single-molecule level. In comparison to

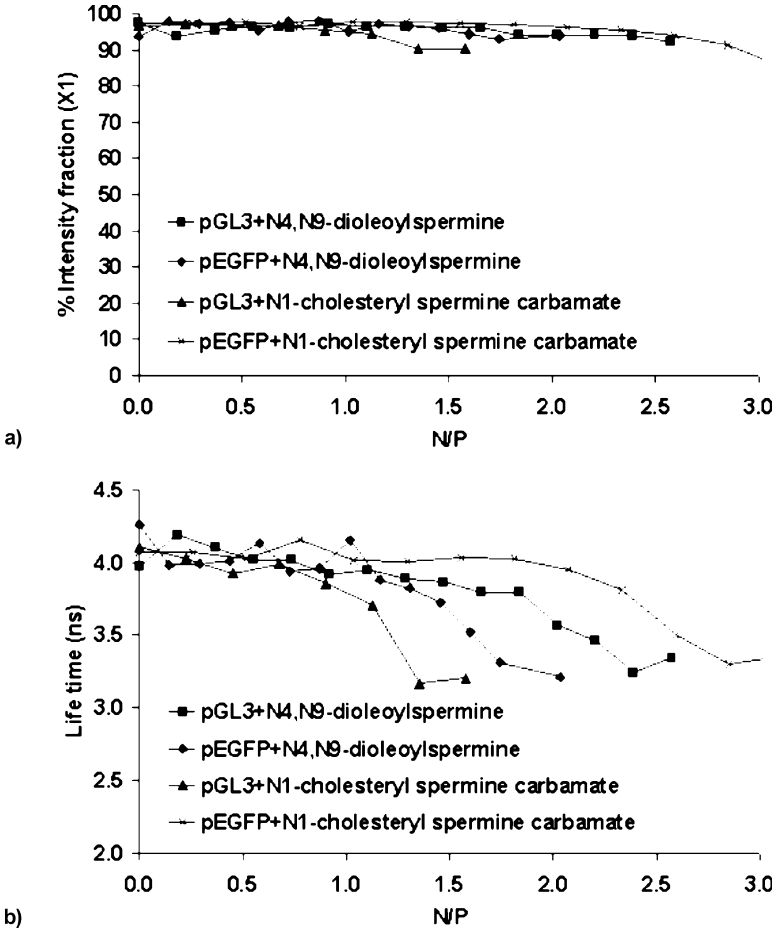

Fig. 19 Intensity fraction **a** of major fluorescent species of DNA-bound PG shows there is no change of the intensity fraction of the major population (4.0-ns dye species) during the DNA condensation process. **b** Lifetime changes (4.0-ns dye species) during the DNA-condensation process.

other DNA markers, the PG used in our FCS study has several advantages: it does not change the hydrodynamic properties of DNA, and it does not influence the lipopolyamine concentrations necessary for condensation. Additionally, due to its high brightness, PG requires tenfold lower staining when compared with previously used markers. PG has a higher affinity than EthBr and other related dyes for dsDNA, in part because of the polyamine moiety structural modification which efficiently forms salt bridges with DNA phosphate anions; taken together with DNA intercalation, this is known as biphasic binding. Finally, the count rate is practically invariant in the condensation process, indicating that dye release does not interfere with the condensation process. As

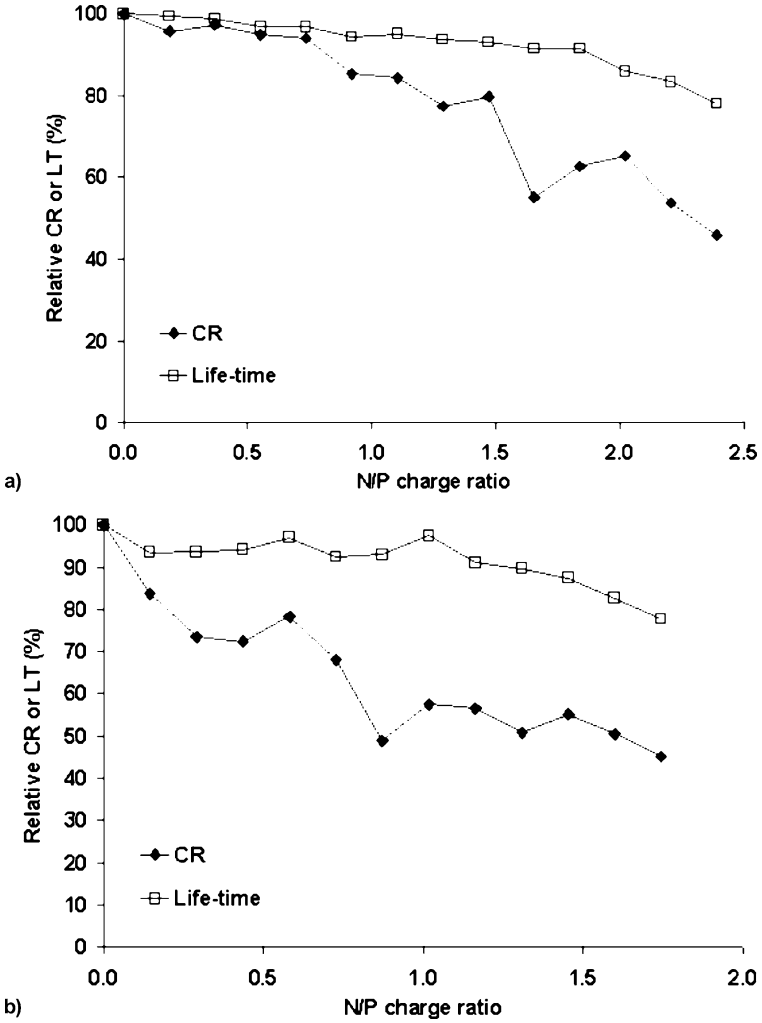

Fig. 20 Lifetime and CR change during the DNA condensation process of **a** pGL3 + N^4,N^9-dioleoylspermine and **b** pEGFP + N^4,N^9-dioleoylspermine

demonstrated using two newly designed lipopolyamines, FCS directly visualizes the condensation process by tracking changes in diffusion coefficients and PNs. In the experiments reported herein, the PN value, which is the most accurate read-out parameter of a FCS experiment, gives quantitative information on the packing density of DNA–lipopolyamine aggregates. Thus, direct information on the quality of condensing molecules can be derived. From this analytical platform, FCS provides detailed information on and insight into DNA and its interaction with gene carriers, which is crucial in the development of safe and effective non-viral gene delivery vectors.

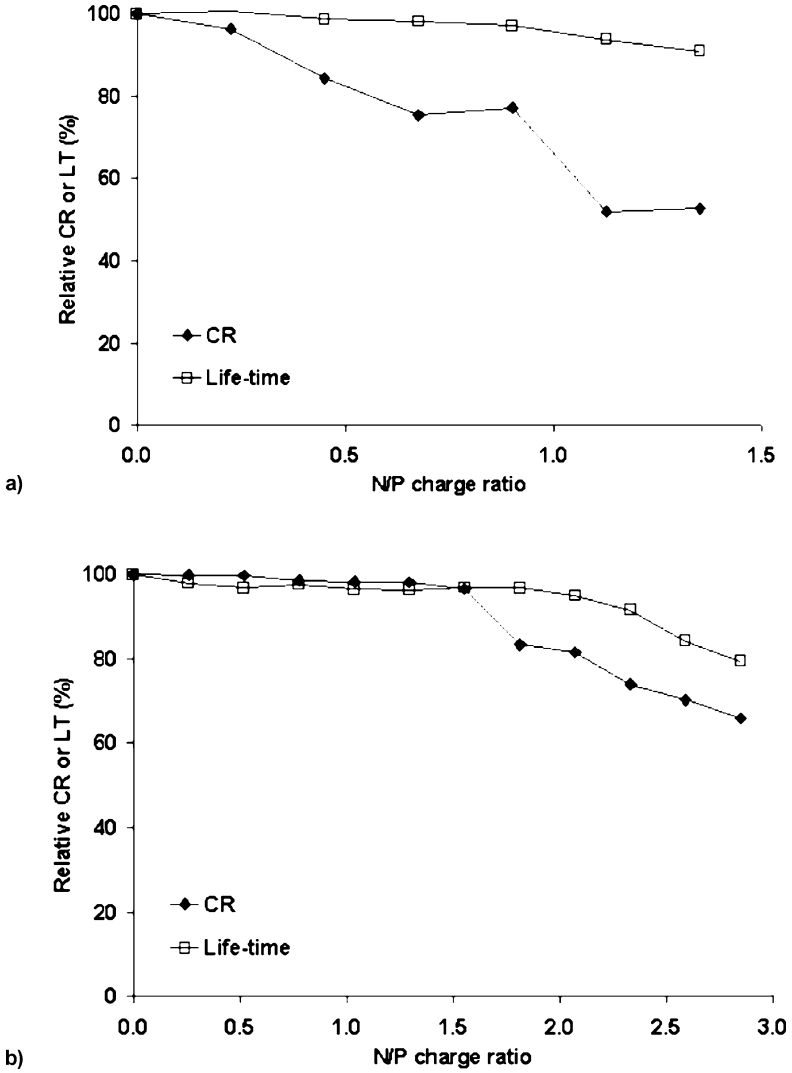

Fig. 21 Lifetime and CR change during the DNA condensation process of **a** pGL3 + N^1-cholesteryl spermine carbamate and **b** pEGFP + N^1-cholesteryl spermine carbamate

In this study, the ConfoCor I set-up upgraded with TimeHarp 200 was used. It offers access to simultaneous lifetime and FCS analysis (TTTR data format). pGL3 and pEGFP condensation with N^4,N^9-dioleoylspermine and N^1-cholesteryl spermine carbamate were used as models. We were able to define the fluorescent signalling behaviour of PG through the process from dye binding to dye release, and then dye quenching. Dye release was suggested as the indicator for DNA conformational change, but not for nanoparticle formation.

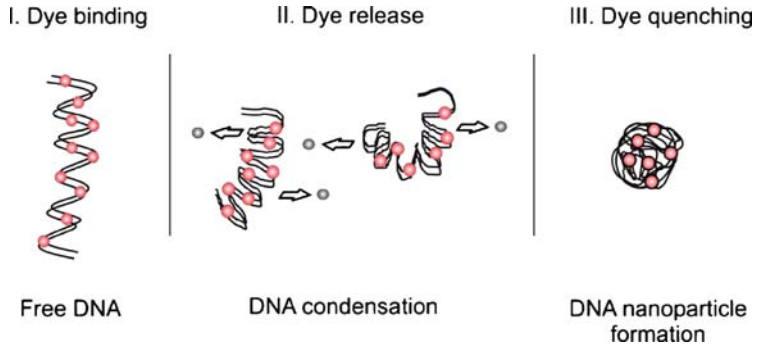

Fig. 22 PG behaviour through the DNA condensation process

Dye quenching, through the observation of lifetime change, is a more important event accurately and sensitively reporting that a single nanoparticle exists.

Acknowledgements We acknowledge support of the Ministry of Education of the Czech Republic via grant LC06063 (AB, MH), the Academy of Sciences of the Czech Republic via grant IAA400400621 (TK), and the Universities UK for an ORS award (partial studentship support to N.A.).

References

1. Bloomfield VA (1991) Biopolymers 31:1471–1481
2. Zabner J, Fasbender AJ, Moninger T, Poellinger KA, Welsh MJ (1995) J Biol Chem 270:18997–19007
3. Bloomfield VA (1996) Curr Opin Struct Biol 6:334–341
4. Bloomfield VA (1997) Biopolymers 44:269–282
5. Godbey WT, Wu KK, Mikos AG (1999) Proc Natl Acad Sci USA 96:5177–5181
6. Wiethoff CM, Middaugh CR (2003) J Pharm Sci 92:203–217
7. Blagbrough IS, Geall AJ, Neal AP (2003) Biochem Soc Trans 31:397–406
8. Thompson NL (1991) Fluorescence correlation spectroscopy. In: Lakowicz JR (ed) Topics in fluorescence spectroscopy. Kluwer, New York, p 337
9. Eigen M, Rigler R (1994) Proc Natl Acad Sci USA 91:5740–5747
10. Walter NG, Schwille P, Eigen M (1996) Proc Natl Acad Sci USA 93:12805–12810
11. Welz C, Fahr A (2001) Appl Spectrosc Rev 36:333–397
12. Rigler R, Elson ES (2001) Fluorescence correlation spectroscopy: theory and applications. Springer, Berlin
13. Enderlein J (2004) Single molecule spectroscopy: basics and applications. In: Hof M, Hutterer R, Fidler V (eds) Fluorescence methods and applications: advanced methods and their applications to membranes, proteins, DNA, and cells. Springer, Berlin Heidelberg, pp 104–122
14. Brock R (2004) Fluorescence correlation spectroscopy in cell biology. In: Hof M, Hutterer R, Fidler V (eds) Fluorescence methods and applications: advanced methods and their applications to membranes, proteins, DNA, and cells. Springer, Berlin Heidelberg, pp 245–262

15. Geall AJ, Blagbrough IS (2000) J Pharm Biomed Anal 22:849–859
16. Bjorling S, Kinjo M, Foldes-Papp Z, Hagman E, Thyberg P, Rigler R (1998) Biochemistry 37:12971–12978
17. Lukacs GL, Haggie P, Seksek O, Lechardeur D, Freedman N, Verkman AS (2000) J Biol Chem 275:1625–1629
18. Benda A, Hof M, Wahl M, Patting M, Erdmann R, Kapusta P (2005) Rev Sci Instrum 76:033106
19. Magde D, Webb WW, Elson E (1972) Phys Rev Lett 29:705
20. Magde D, Elson EL, Webb WW (1974) Biopolymers 13:29–61
21. Kral T, Langner M, Benes M, Baczynska D, Ugorski M, Hof M (2002) Biophys Chem 95:135–144
22. Kral T, Hof M, Langner M (2002) Biol Chem 383:331–335
23. Jurkiewicz P, Okruszek A, Hof M, Langner M (2003) Cell Mol Biol Lett 8:77–84
24. Kral T, Hof M, Jurkiewicz P, Langner M (2002) Cell Mol Biol Lett 7:203–211
25. Van Rompaey E, Engelborghs Y, Sanders N, De Smedt SC, Demeester J (2001) Pharm Res 18:928–936
26. Sobell HM, Tsai CC, Jain SC, Gilbert SG (1977) J Mol Biol 114:333–365
27. Manning GS (1978) Q Rev Biophys 11:179–246
28. Nordmeier E (1992) J Phys Chem 96:6045–6055
29. Singer VL, Jones LJ, Yue ST, Haugland RP (1997) Anal Biochem 249:228–238
30. Millard PJ, Roth BL, Thi HPT, Yue ST, Haugland RP (1997) Appl Environ Microbiol 63:2897–2905
31. Zipper H, Brunner H, Bernhagen J, Vitzthum F (2004) Nucleic Acids Res 32:e103
32. Eriksson M, Karlsson HJ, Westman G, Akerman B (2003) Nucleic Acids Res 31:6235–6242
33. Petty JT, Bordelon JA, Robertson ME (2000) J Phys Chem B 104:7221–7227
34. Zipper H, Buta C, Lammle K, Brunner H, Bernhagen J, Vitzthum F (2003) Nucleic Acids Res 31:e39
35. Yan X, Grace WK, Yoshida TM, Habbersett RC, Velappan N, Jett JH, Keller RA, Marrone BL (1999) Anal Chem 71:5470–5480
36. Yan XM, Habbersett RC, Yoshida TM, Nolan JP, Jett JH, Marrone BL (2005) Anal Chem 77:3554–3562
37. Beach L, Schweitzer C, Scaiano JC (2003) Org Biomol Chem 1:450–451
38. Schweitzer C, Scaiano JC (2003) Phys Chem Chem Phys 5:4911–4917
39. Tsai JT, Furstoss KJ, Michnick T, Sloane DL, Paul RW (2002) Biotechnol Appl Biochem 36:13–20
40. Choi JS, Nam K, Park J, Kim JB, Lee JK, Park J (2004) J Control Release 99:445–456
41. Kasper FK, Seidlits SK, Tang A, Crowther RS, Carney DH, Barry MA, Mikos AG (2005) J Control Release 104:521–539
42. Singh R, Pantarotto D, McCarthy D, Chaloin O, Hoebeke J, Partidos CD, Briand JP, Prato M, Bianco A, Kostarelos K (2005) J Am Chem Soc 127:4388–4396
43. Kral T, Widerak K, Langner M, Hof M (2005) J Fluoresc 15:179–183
44. Lumma D, Keller S, Vilgis T, Radler JO (2003) Phys Rev Lett 90:218301(1)–218301(2)
45. Kleideiter G, Nordmeier E (1999) Polymer 40:4025–4033
46. Yoshikawa K, Yoshikawa Y, Kanbe T (2002) Chem Phys Lett 354:354–359
47. McLaggan D, Adjimatera N, Blagbrough IS, Sepčić K, Jaspars M, MacEwan DJ, Scott RH (2006) BMC Biotechnol 6:6
48. Ahmed OAA, Pourzand C, Blagbrough IS (2006) Pharm Res 23:31–40
49. Adjimatera N, Neal AP, Blagbrough IS (2004) Fluorescence techniques in non-viral gene therapy. In: Hof M, Hutterer R, Fidler V (eds) Fluorescence methods and applications:

advanced methods and their applications to membranes, proteins, DNA, and cells. Springer, Berlin Heidelberg, pp 201–228
50. Ahmed OAA, Adjimatera N, Pourzand C, Blagbrough IS (2005) Pharm Res 22:972–80
51. Blagbrough IS, Adjimatera N, Ahmed OAA, Neal AP, Pourzand C (2004) Spermine and lipopolyamines as gene delivery agent. In: Beadle DJ, Mellor IR, Usherwood PNR (eds) Neurotox'03: neurotoxicological targets from functional genomics and proteomics. Society of Chemical Industry, London, pp 147–159
52. Geall AJ, Taylor RJ, Earll ME, Eaton MAW, Blagbrough IS (2000) Bioconjug Chem 11:314–326
53. Cosa G, Focsaneanu KS, McLean JRN, McNamee JP, Scaiano JC (2001) Photochem Photobiol 73:585–599